

First Detection of an Ultracool Dwarf at 340 MHz: VLITE Observations of EI Cancri AB

MICHELE L. SILVERSTEIN  ^{1,*} TRACY E. CLARKE  ¹ WENDY M. PETERS  ¹ EMIL POLISENSKY  ¹,
 JACKIE VILLADSEN  ² AND JORDAN M. STONE  ¹

¹ Naval Research Laboratory, 4555 Overlook Avenue SW, Washington, DC 20375, USA

² Department of Physics & Astronomy, Bucknell University, Lewisburg, PA, USA

ABSTRACT

Magnetically driven phenomena such as flaring events and aurorae lead ultracool dwarfs to emit at radio frequencies. Despite decades of scrutiny, a comprehensive physical understanding of their radio emission at different frequencies remains elusive, spurring on additional study of these complex objects. The VLA Low-band Ionosphere and Transient Experiment (VLITE) is a commensal instrument operating at 340 MHz on the Very Large Array. A key advantage of 340 MHz observations is their sensitivity to circumstellar disks and planets at understudied distances from the stellar disk, intermediate between GHz and low MHz sensitivities. Hard-to-find coronal mass ejections are also predicted to be detectable at 340 MHz. However, this frequency regime is relatively unprobed in ultracool dwarf studies, with few searches and no published detections to date. Here we highlight our investigation of the nearby M7-M7 binary, EI Cancri. EI Cancri AB is magnetically active, yet has an uncharacteristically long 83-day candidate rotation period within the system. With the VLITE detection of the EI Cancri system, we present the first ever detection of ultracool dwarf emission at 340 MHz.

1. INTRODUCTION

1.1. Overview

Ultracool dwarfs (UCDs) are comprised of brown dwarfs and the smallest main sequence stars, with spectral types M7 and later (Kirkpatrick et al. 1997). These objects are fully convective and therefore lack a tachocline, yet much of our understanding of magnetic processes in solar-type stars has hinged on this structure. Although this has left a gap in our understanding of the drivers of magnetic phenomena in UCDs, recent studies have begun to reveal the dynamos and processes behind UCD magnetic activity (e.g., Williams et al. 2014; Cook et al. 2014; Kao et al. 2016). Overviews and recent studies of dynamos and magnetic fields in UCDs, including those in radio, can also be found in, e.g., Tang et al. (2022); Kavanagh et al. (2024); Couperus et al. (2025b).

The vast majority of radio studies of UCDs have been at GHz frequencies (e.g., Berger 2006; Route & Wolszczan 2013; Kao et al. 2019; Pineda & Villadsen 2023; Ortiz Ceballos et al. 2024), with additional focus at $\lesssim 200$ MHz (e.g., Callingham et al. 2021; Huang et al. 2024) using the LOw-Frequency ARray (LOFAR; van Haarlem et al. 2013) and Murchison Widefield Array (GaLactic and Extragalactic All-sky Murchison Widefield Array survey eXtended; GLEAM-X; Hurley-Walker et al. 2022). Fewer studies have been performed at ~ 340 MHz, the main frequency we examine in this study. Jaeger et al. (2011) observed two UCDs, TVLM 513-46546 and 2MASS J0036+182110, with the VLA at P-band (224-480 MHz), centered at ~ 330 MHz. Observations spanned multiple rotations of the UCDs and resulted in non-detections. Crosley & Osten (2018a,b) searched for emission from M dwarf binary system EQ Peg also in the VLA P-band and found two events in 44 hours. Villadsen & Hallinan (2019) used the VLA to search for coherent emission across a range of frequencies including P-band from 5 active M dwarfs, and found that emission was less likely to be detected in P-band than at GHz frequencies. The paucity of 340 MHz frequency observations to date inherently increases the value of additional studies, with the possibility of detecting orbiting bodies, coronal mass ejections, or flares in areas of phase space unprobed by those corresponding to $\lesssim 200$ MHz and GHz frequencies.

Analogously to the Jupiter system, interaction between the stellar magnetic field and an orbiting planet or plasma torus can drive radio emission (see reviews by Callingham et al. 2024; Murphy & Kaplan 2025). Observations at 340 MHz are valuable for their sensitivity to these bodies at distances from the star not covered by other frequencies

* NRC Research Associate

(Dulk 1985). Whereas GHz-frequency emission is mainly tied to the stellar disk and its small-scale magnetic loops, 340 MHz corresponds to the further-out large-scale magnetic field and the outer part of larger small-scale loops (see, e.g., Villadsen & Hallinan 2019). This is in contrast to even lower frequencies, which probe the large-scale magnetic field at even greater distances from the stellar disk (Vedantham et al. 2020). Our 340 MHz observations help fill the “gap” between the stellar surface and distances probed at lower frequencies; if we are blind at this frequency, we may overlook a disk or planet interacting with the large-scale magnetic field. Such detections are key to holistically characterizing the system, with the potential to measure an exoplanetary magnetic field for the first time.

Probing new frequencies can also reveal the diversity of stellar radio burst types and help build towards a classification scheme that includes space weather events; many solar radio bursts are narrow-band, with different burst types dominating at different frequency ranges (Bastian et al. 1998). Villadsen & Hallinan (2019) describe that it is possible to detect Type II or Type III bursts at 340 MHz. These are tied to solar coronal mass ejections (CMEs) or flares in the Sun (Vršnak & Cliver 2008). In other stars, we expect similar emission corresponding to eruptive events propagating through the stellar plasma. Zic et al. (2020) and Mohan et al. (2024) also describe a mechanism for CMEs to present in low-mass stars as Type IV bursts. In other stars, we expect similar emission corresponding to eruptive events propagating through the stellar plasma; the first such stellar Type II candidate was recently observed by Callingham et al. (2025) at 120–165 MHz. Zic et al. (2020) and Mohan et al. (2024) also present sub-GHz observations of stellar Type IV bursts, which in the Sun are well-correlated with post-eruptive coronal reconfiguration. These results motivate continued searches at low and intermediate MHz frequencies to detect additional scarce signatures of CMEs.

In this paper, we report on the discovery of 340 MHz emission from UCD binary EI Cancri AB, marking the first detection of an UCD at this frequency. We demonstrate multi-frequency radio emission in this system spanning over three decades. First we introduce the EI Cancri system in Section 1.2. In Section 2, we describe the observations of EI Cancri using VLITE and results. In Section 3, we discuss the nature of the detected emission. Lastly, in Section 4, we draw our conclusions and describe prospects for future work on this system.

1.2. The EI Cancri System

EI Cancri AB (G 9-38AB, GJ 1116 AB, TIC 197251248 (A) + TIC 471012520 (B)) was first identified as a flare star system by Pettersen (1985). It is comprised of two main sequence M7 stars (Newton et al. 2014) at ~ 5.12 pc (Bailer-Jones et al. 2021), with masses of 0.120 ± 0.014 M_{\odot} and 0.103 ± 0.014 M_{\odot} (Winters et al. 2021) and at a separation of $2.5478'' \pm 0.0003''$ (Tokovinin et al. 2020). Multiple measurements of rotation period have been taken for the system (83 days by Newton et al. (2016) and ~ 10 hours by Jeffers et al. (2018)) with no period conclusively ascribable to either star due to unresolved data (see Section 3.4). With a projected separation of 13 AU, EI Cancri A and B do not have interacting magnetic fields, in line with radio-emitting UCD binaries identified to date (Kao & Pineda 2025). In Table 1, we present fundamental properties and measurements of the EI Cancri system.

Orbital parameters have not been determined for this system, and no exoplanet candidates have been reported to date. Gaia Data Release 3 (DR3; Gaia Collaboration et al. 2016, 2023; Babusiaux et al. 2023) Renormalised Unit Weight Error (RUWE) values for each star of $\gtrsim 1.4$ suggest the system may yet have an additional companion (Lindegren et al. 2018; Belokurov et al. 2020; Stassun & Torres 2021; Gaia Collaboration 2022). However, it is possible that these higher RUWE values stem from the exclusion of an orbital fit in the astrometric solution for these two stars, rather than a third body. Some orbital motion has been seen in Southern Astrophysical Research (SOAR) Telescope speckle data over 2019–2021 (Tokovinin et al. 2020; Vrijmoet et al. 2022, Eliot Vrijmoet, private communication). The system increased by $0.1''$ in separation and rotated 3.6° in position angle; this may be enough motion to account for the high RUWE in both components in Gaia DR3. Speckle observations taken by the aforementioned SOAR speckle team and Robo-AO team (Salama et al. 2022) have yielded no discovery of a third member of the system to date.

The Transiting Exoplanet Survey Satellite (TESS; Ricker et al. 2015) lightcurve of the EI Cancri system shows spot modulation and frequent flares. With a TESS resolution of $21''$ and EI Cancri AB a near-equal-mass binary, flux cannot be disentangled between the two stars, so the source(s) of these magnetic activity signatures cannot be distinguished between them. As we’ll discuss in Section 3, magnetic phenomena can lead to other types of emission, such as excess UV and X-ray flux (see Table 1), in addition to the radio emission presented in this work.

Previous detections of radio emission from EI Cancri AB have been made from 855.5 MHz to 5 GHz and 90–220 GHz, as shown in Table 2. However, no known studies have been performed to interpret these data and put them in context with the known magnetic properties of the system.

Table 1. Basic Information

Property	EI Cancri A	Error	EI Cancri B	Error	Reference
Common Names	GJ 1116 A	...	GJ 1116 B
	G 9-38A	...	G 9-38B
	TIC 197251248	...	TIC 471012520
Astrometry and Kinematics					
RA (epoch 2016.0; hms)	08 ^d 58 ^m 14.206 ^s	< 0.001 ^s	08 ^d 58 ^m 14.086 ^s	< 0.001 ^s	Gaia DR3
Dec (epoch 2016.0; dms)	+19° 45' 46.655"	< 0.001"	+19° 45' 45.284"	< 0.001"	Gaia DR3
Parallax (mas)	194.1443	0.1228	196.2619	0.1976	Gaia DR3
Distance (pc)	5.1499	+0.0027 -0.0039	5.0939	+0.0062 -0.0051	Bailer-Jones et al. (2021)
Total Proper Motion (mas yr ⁻¹)	773.574	...	937.770	...	Gaia DR3
RA Proper Motion (mas yr ⁻¹)	-767.060	0.122	-937.133	0.190	Gaia DR3
Dec Proper Motion (mas yr ⁻¹)	-100.176	0.083	-34.559	0.138	Gaia DR3
Gaia RUWE	2.574	...	3.539	...	Gaia DR3
AB Separation (2019.9474; arcsec)	2.5478	0.0003	Tokovinin et al. (2020)
AB Position Angle (2019.9474; deg)	244.8	0.3 mas	Tokovinin et al. (2020)
Photometry					
Gaia G (mag)	11.9663	0.0029	12.4856	0.0030	Gaia DR3
Gaia BP (mag)	14.3240	0.0045	15.0630	0.0054	Gaia DR3
Gaia RP (mag)	10.5470	0.0058	11.0246	0.0068	Gaia DR3
2MASS K _s (mag)	6.889	0.023	2MASS; combined
GALEX NUV (mag)	19.4572	0.1112	Bianchi et al. (2017); combined
GALEX FUV (mag)	20.7616	0.2886	Bianchi et al. (2017); combined
ROSAT flux (10 ⁻¹² erg cm ⁻² s ⁻¹)	2.9770	Boller et al. (2016); combined
L _X (ROSAT; 10 ²⁷ erg s ⁻¹)	9.2647	Boller et al. (2016); combined
Derived Properties					
Spectral Type	M7	...	M7	...	Newton et al. (2014)
Mass (M _⊕)	0.120	0.014	0.103	0.014	Winters et al. (2021)
Radius (R _⊕)	0.148	0.013	0.132	0.013	Pineda et al. (2021) M-R Relation [†]
EW _{Hα} (Å)	-5.719	0.044	Newton et al. (2017); combined
L _{Hα} /L _{bol}	1.027 × 10 ⁻⁴	Newton et al. (2017); combined
P _{rot,combined} (days) [‡]	83.270	Newton et al. (2016); combined
P _{rot} (days) [‡]	112.74	...	115.53	...	Newton et al. (2017) eqn. 6
vsini (km s ⁻¹) [‡]	16.70	0.64	Jeffers et al. (2018); combined

[†] <https://github.com/jspineda/stellarprop>[‡] Note a discrepancy between periods from Newton et al. (2016, 2017) and from Jeffers et al. (2018); see Section 3.4.

Here we deepen the radio characterization of this system by extending down to the yet unexplored 340 MHz regime, revealing the first UCD detections at this frequency and interpreting the cumulative radio detections of this system to date.

2. OBSERVATIONS AND RESULTS

2.1. VLITE

The VLA Low-band Ionosphere and Transient Experiment (VLITE)³ is a commensal instrument on the Karl G. Jansky Very Large Array (VLA). Operating at a central frequency of 340 MHz, with an effective 40 MHz bandwidth, it records and correlates data during nearly all standard VLA observations at GHz frequencies, also called the primary frequencies. Science operations began with 10 antennas in 2014 November, and the system currently operates on 18

³ <https://vlite.nrao.edu>

Table 2. Archival Radio Data

Survey/Facility	Freq. (MHz)	Resolution	Component	Flux Density (mJy)	Error (mJy)	Epoch (yr)	Ref ...	Brightness (This work; K)	Temp. (K)	Error (This work; K)
NVSS*	1400	45''	U	3.3	0.4	1993.833	C98
FIRST†	1400	5''	U	3.67	0.151	1998.775	B95, H15
VLA	5000	~1''-10''	U	1.482	0.082	2005.671233	B09
VLITE	340	~4''	U	2.70	0.35	2018.3152329	this work
ACT	220 GHz	1'	U	103	31	2018.8718379	L23
ACT	150 GHz	1'	U	197	9	2018.8718379	L23
ACT	90 GHz	1'	U	269	9	2018.8718379	L23
VLASS 1	3000	~ 2.5''	A	0.82	0.18	2019.2822444	L20, this work	5.50×10^{11}	1.55×10^{11}	
VLASS 1	3000	~ 2.5''	B	1.082	0.189	2019.2822444	L20	8.92×10^{11}	2.35×10^{11}	
ASKAP 02-03hour	855.5	~ 15''	U	6.87	0.05	2020.2936	M20, Dr24
ASKAP	855.5	~ 15''	U	1.45	0.02	2020.2938	M20, Dr24
ASKAP RACS-MID	1367.5	~ 10''	U	2.2	0.5	2021.0293	M20, Du24, Dr24
ASKAP	1367.5	~ 10''	U	3.7	0.5	2021.0431	M20, Dr24
VLASS 2	3000	~ 2.5''	A	1.269	0.130	2021.877854	L20	8.51×10^{11}	1.73×10^{11}	
VLASS 2	3000	~ 2.5''	B	1.092	0.126	2021.877854	L20	9.01×10^{11}	2.06×10^{11}	
ASKAP RACS-HIGH	1655.5	~ 8''	U	1.4	0.3	2021.9940	M20, Dr24, Du25
ASKAP	855.5	~ 15''	U	2.6	0.2	2022.4066	M20, Dr24
ASKAP	855.5	~ 15''	U	1.5	0.2	2022.4093	M20, Dr24
ASKAP	943.5	~ 15''	U	5.2	0.4	2023.9886	M20, Dr24
ASKAP	943.5	~ 15''	U	5.6	0.4	2023.9912	M20, Dr24
ASKAP	943.5	~ 15''	U	4.1	0.1	2024.0265	M20, Dr24
ASKAP	1367.5	~ 10''	U	2.42	0.07	2024.1602	M20, Dr24
VLASS 3	3000	~ 2.5''	A	1.413	0.161	2024.333561	L20, this work	9.48×10^{11}	1.98×10^{11}	
VLASS 3	3000	~ 2.5''	B	1.706	0.165	2024.333561	L20, this work	1.41×10^{12}	3.09×10^{11}	

* Note that there is a $\sim 7''$ separation between NVSS and Gaia proper-motion shifted coordinates. This separation is mostly in Dec and comparable to the NVSS Dec error of $5.5''$. C98 highlight a lower reliability in optically identifying sources weaker than 5 mJy and demonstrate that position uncertainties smaller than $30''$ have a false alarm probability of ~ 0.01 . We believe this detection likely corresponds to emission in the EI Cancri system, but caution the reader of these uncertainties.

U = unclear whether the flux comes from EI Cancri A, B or both.

NVSS: National Radio Astronomy Observatory (NRAO) Very Large Array (VLA) Sky Survey, FIRST: Faint Images of the Radio Sky at Twenty-centimeters, ACT: Atacama Cosmology Telescope, VLASS: VLA Sky Survey, ASKAP: Australian Square Kilometre Array Pathfinder, RACS: Rapid ASKAP Continuum Survey

C98=Condon et al. (1998), B95=Becker et al. (1995), H15=Helfand et al. (2015), B09=Bower et al. (2009), L23=Li et al. (2023), L20=Lacy et al. (2020), M20=McConnell et al. (2020), Dr24=Driessen et al. (2024) & <https://radiostars.org/>, Du24=Duchesne et al. (2024), Du25=Duchesne et al. (2025)

† Strangely, FIRST emission is detected between the proper-motion-corrected coordinates of each star, but is point-like rather than elongated, suggesting that it comes from only one source.

antennas. VLITE collects more than 6000 hrs/yr of data. The wide field of view (2.45° FWHM) provides measurements of sources over a large sky area around each primary science target position.

Data are typically stored in blocks containing all data acquired within a 24-hour period. Due to its commensal nature, the VLITE database has a non-uniform distribution of depth of sky coverage. Data are processed on a daily basis, with each primary observing frequency processed separately due to variations in the instrumental response. A dedicated calibration and imaging pipeline relies on a series of standard tasks in the `Obit` (Cotton 2008) and `Astronomical Image Processing System` (AIPS) (Greisen 2003) software packages. Correction of delays, frequency-dependent complex gains, and frequency-independent complex gains are made using observations of one of six primary calibrators (3C48, 3C138, 3C147, 3C286, 3C295, and or 3C380), using models which are set to the `Perley & Butler` (2017) flux scale. After editing to remove radio frequency interference (RFI), all data are phase calibrated to a sky model based on the National Radio Astronomy Observatory (NRAO) VLA Sky Survey (NVSS; Condon et al. 1998). The data are imaged using the `Obit` task ‘MFImage.’ Calibrated visibilities and final images are stored in archives at the Naval Research Laboratory (NRL). For more details on standard VLITE processing, please see Polisensky et al. (2016).

Source detection is performed using the VLITE Database Pipeline (VDP; [Polisensky et al. 2019](#)), which utilizes PyBDSF ([Mohan & Rafferty 2015](#)) source extraction to catalog sources with signal-to-noise ratios (S/N) > 5 . VDP calculates and applies calibration for VLITE’s elaborate primary beam response ([Polisensky et al. 2024](#)) and stores end data products in a Structured Query Language (SQL) database.

Key to the current study is deployment of a “time-chopping” methodology to sample the VLITE data at different durations and cadences. Using the same software tools used in the imaging pipeline, we “chop” the data into a series of shorter-time images from the larger whole. This chopping of long-duration images (the longest being ~ 7 hours) into shorter cadences enables us to search for shorter events.

2.2. *EI Cancri in VLITE*

To search for radio emission resolved between the binary components of EI Cancri, we focus on A-configuration observations, which provide the highest angular resolution available ($\sim 5''$). Since the 2017 upgrade to 18 antennas that enabled VLITE imaging in A configuration, 111 images include EI Cancri within the field of view. These observations span 2018 March 2 to 2024 December 19. During this time, the EI Cancri system moves $8.7''$ across the sky; we use Gaia DR3 proper-motion-shifted coordinates for the EI Cancri system at the midpoint time of the VLITE observations ($RA = 08^h 58^m 13.81^s$, $Dec = +19^\circ 45' 45.59''$, epoch = 2021.62839). All observations of EI Cancri are 0.874° from pointing center, which corresponds to a common calibrator, J0854+2006. There are no data in which EI Cancri is the intended target of the Cassegrain antennae observers; these are serendipitous detections outside the field of view of the primary GHz frequency observations.

Emission from EI Cancri at 340 MHz is detected in a deep archival image from VLITE observations taken during project GG083, which observed the nearby blazar OJ 287 at 22 GHz. The VLITE image of EI Cancri, shown in the left panel of Figure 1, includes 7.036 hours of on-source time, spread over a total of 28 hours on 2018 April 26 to 2018 April 27 (see also Table 2). The image has a resolution of $3.9'' \times 3.8''$ at a position angle of 66° , and a local rms noise of 0.35 mJy bm^{-1} . To determine the astrometric accuracy of the image, we compare the measured positions of 82 compact point sources with $S/N > 10$ to their positions in the 1400 MHz FIRST survey ([Becker et al. 1995](#)), which has a comparable resolution ($5''$) to the VLITE image and a measured astrometric accuracy of $< 0.05''$. The median astrometric accuracy of the VLITE sources relative to FIRST is $0.04''$, comparable to the survey accuracy.

The right panel of Figure 1 shows a small region of the image centered on the detected radio emission. The positions of EI Cancri A and B at the time of the observation are labeled. The VLITE source centroid is closest to EI Cancri A, with an offset of $0.64''$ while the offset to EI Cancri B is $2.05''$. The shape of the time-averaged position measured in this long observation matches that of a point source rather than an unresolved binary, as would be expected if the emission was uniformly distributed between EI Cancri A and B. We do not have strong reason to believe there is a third UCD companion in the system generating the emission (see Section 1.2). Given the resolution of $\sim 4''$ and our measured astrometric accuracy, the VLITE position is most consistent with an association with EI Cancri A.

Due to the prevalence of shorter-timescale optical flares, the long 7-hour image likely contains multiple shorter outbursts; therefore, to search for time-resolved radio emission and identify shorter events, we split the full 111-image dataset into smaller time bins. With no UCD detections in this frequency to date, we guide our cadence selection using optical flare timescales, even if there is some uncertainty in their physical connection (i.e. radio emission may not be from flares). We choose a 10-minute cadence, in line with findings by [Pettersen \(1985\)](#) of about five flares per hour. The result is a total of 574 images, totaling ~ 23 hr on source. Each image was processed using VDP in a non-standard mode that catalogs sources with $S/N > 3$ to identify potential low-significance detections of EI Cancri.

We identified 42 sources within $10''$ of the proper motion-corrected position of EI Cancri. At these low S/N levels, spurious noise detections are a concern. To quantify the likelihood of false associations, we conducted a statistical analysis assuming all detections are randomly distributed artifacts. For each image, the expected number of false positives is the product of the $10''$ association solid angle Ω_* and the areal density of detections, n_i/Ω_{FoV} , where n_i is the number of sources and $\Omega_{\text{FoV}} = 0.25 \text{ deg}^2$ is the image field of view. Summing over all N images yields the expected number of false associations:

$$\lambda = \sum_{i=1}^N \Omega_* \frac{n_i}{\Omega_{\text{FoV}}} \quad (1)$$

We detected 38 associations with S/N between 3 and 4, consistent with the expected 38.7 false positives. For $S/N > 4$, we detected 4 associations, compared to 2.1 expected false positives. Visual inspection of the four high- S/N

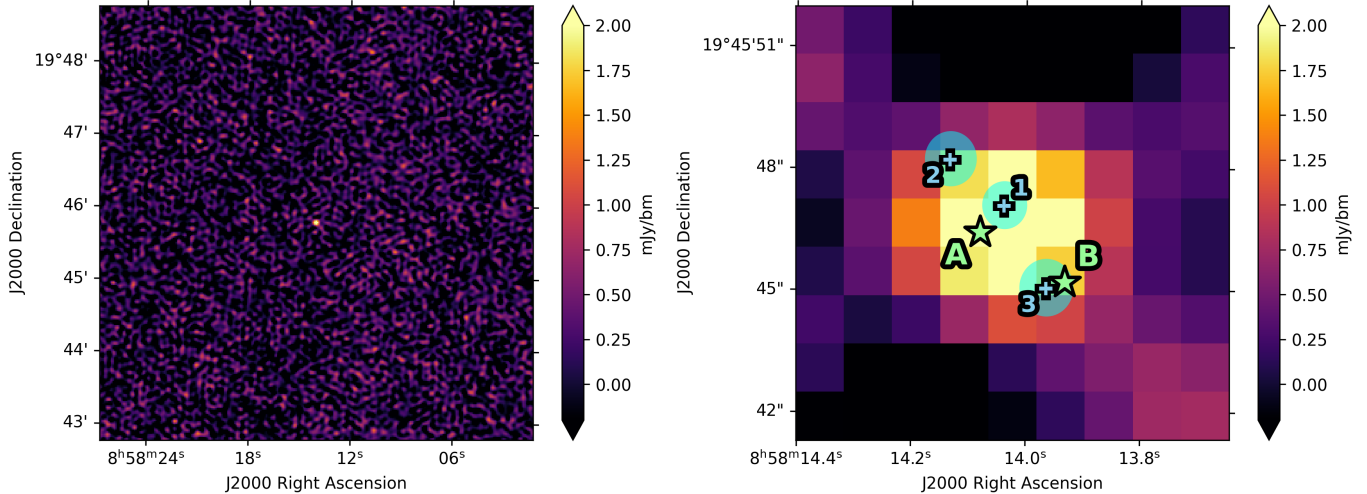


Figure 1. Left: VLITE detection of EI Cancri on 2018 April 26 from an image with 7 hours on source across a 28-hour duration. The image has a pixel scale of $1.2'' \text{ pixel}^{-1}$ and a resolution of $3.9'' \times 3.8''$. The stellar binary is prominently detected with a peak flux of $2.70 \pm 0.35 \text{ mJy bm}^{-1}$ and $\text{S/N} = 7.71$. Right: Zoom-in on the detection. The positions of the stellar components are shown by the star symbols, corrected for proper motion. The positions of the three individual detections in the time-chopped (10 minute) images are marked with '+' symbols, with shaded light blue circles representing 1σ positional errors. Table 2 places the 7-hour event in context with other archival detections, and the three 10-minute events are further described in Table 3.

candidates revealed one likely artifact. The remaining three significant events all occurred on 2018 April 27, during the 7-hour interval when EI Cancri was detected.

To confirm the events, search for the times of highest S/N, and map out the light curve, we applied boxcar smoothing to the 7-hour dataset, such that each 10-minute image overlaps the next by 9 minutes. Each bin included at least 6.5 minutes of time on-source, with the majority containing a full 10 minutes. With this methodology, we are able to identify the time with the highest S/N for each event, presented in Table 3, with positions displayed in the right panel of Figure 1. These three events have peak emissions of 14.4 mJy, 10.1 mJy, and 10.3 mJy at UT = 00:09, 02:48, and 03:41, respectively. In all cases, the emission is spatially unresolved. We adopt the fitted peak brightness as the source flux density, because the fitted sizes and total fluxes of weak sources in VLITE data are biased to larger values (Polisensky et al. 2024).

At low radio frequencies, the ionosphere introduces a refractive phase error which can be removed by calibrating to a sky model with known source positions; for VLITE we use the NVSS for this purpose (Polisensky et al. 2016). However, on baselines longer than the projected scale of structures in the ionosphere, the field-of-view over which this position-independent calibration is valid, or isoplanatic patch, may be less than the desired area of the image. In VLITE archival data we see small position-dependent offsets only in the largest VLA configuration (A configuration). Generally the isoplanatic patch is $\gtrsim 1.0^\circ$, and typical errors are $\lesssim 2 - 3''$ on timescales of minutes. Over longer observations, such as the 7 hours of data in the original archival detection image, the net result of leaving the direction-dependent ionospheric phases uncorrected is to slightly smear the sources, leading to a decrease in the peak flux, but an accurate total flux and position (Cohen et al. 2003).

Unfortunately, 10 minutes is not sufficient to average out the ionospheric effects, so the astrometric uncertainty is expected to be larger than in the 7 hour image analyzed previously. Due to the decreased sensitivity of the shorter images, we do not detect enough sources to robustly analyze the astrometric errors in each image individually as we did for the 7 hour image. Instead, we estimate the position errors by measuring the position shifts of 12 point sources within a radius of 0.5° of EI Cancri in all of the 10 minute images, for a total of 517 detections. The 1σ uncertainty is $0.53''$ in RA and $0.38''$ in Dec, with a small number of outliers, roughly 1% of the total, at offsets $\sim 2''$.

In the right panel of Figure 1, the positions of the three ten-minute detections are indicated with blue crosses. A shaded region is shown around each detection, representing the 1σ positional uncertainty derived from the fitting uncertainty, ionospheric positional variations, and astrometric calibration errors, added in quadrature. Each detection has a point-like profile. The position of burst 3 matches that of EI Cancri B within the estimated errors. Bursts 1 and

2 are both closer to EI Cancri A, although neither matches the star's position within the estimated uncertainty. If both stars are emitting then it would explain the relatively central position of the 7-hour detection between EI Cancri A and B. Additional follow-up observations at this frequency with direction-dependent calibration would be necessary to confirm whether both stars are active as suggested by these results. The source coordinates and their 1σ positional uncertainties, derived from the Gaussian fits, are listed in Table 3 alongside the times and flux densities.

Table 3. VLITE Detections

Event #	Date and Midtime	RA	σ_{RA}	Dec	σ_{Dec}	Flux Density	Error	Time	On-source	S/N	T_B	Error
...	...	(hms)	(arcsec)	(dms)	(arcsec)	(mJy)	(mJy)	(sec)	...	\cdots	(10^{12} K)	(10^{12} K)
1	2018-04-27 UT 00:09:00	08 ^h 58 ^m 14.04 ^s	0.25	+19°45'47.11"	0.20	14.4	3.2	600	5.7	9.7	2.7	
2	2018-04-27 UT 02:48:00	08 ^h 58 ^m 14.14 ^s	0.34	+19°45'48.12"	0.42	10.1	2.5	600	4.9	6.8	2.1	
3	2018-04-27 UT 03:41:00	08 ^h 58 ^m 13.96 ^s	0.27	+19°45'44.73"	0.47	10.3	2.6	600	4.9	6.9	2.1	

To determine the nature of the emission, we calculate the stellar disk-averaged brightness temperature (T_B) of each event (henceforth “brightness temperature”). Brightness temperature in K is determined as a function of flux density (S), distance to the star (d), and size of the emitting region (r):

$$T_B = 2.8156 \times 10^{-7} \cdot S \left(\frac{d}{r} \right)^2 \quad (2)$$

for S in mJy, $\frac{d}{r}$ unitless, and adoption of the stellar radius of EI Cancri A in units of R_\odot for r . We estimate stellar radius by substituting masses from [Winters et al. \(2021\)](#) into the relation from [Pineda et al. \(2021\)](#). Derived brightness temperatures from VLITE data $\gtrsim 10^{12}$ K indicate a coherent emission mechanism ([Dulk 1985; Melrose 1991](#)). All of our VLITE detections meet this criterion. However, at 340 MHz, the radius of emission could be from large magnetic loops as far from the stellar surface as the source surface radius, where the magnetic field lines become open. This radius could be expected to be on the order of $5 R_*$ ([Vidotto et al. 2014](#)). In this case, brightness temperature is smaller by a factor of 25, below the $\sim 10^{12}$ K coherent emission threshold for each event.

Our measured radio fluxes and archival ROSAT X-ray luminosity land very close to the Güdel-Benz empirical relation (GBR) ([Drake et al. 1989; Guedel & Benz 1993; Benz & Guedel 1994](#)). This could be taken as evidence of incoherent, gyrosynchrotron emission. However, there is evidence that low-frequency, strongly-polarized emission, previously presumed to be coherent, adheres to the GBR in some cases (e.g., RS CVns; [Vedantham et al. 2022](#)). Our result suggests a unique property of the EI Cancri system given previous LOFAR observations which found that low-frequency radio emission from M dwarfs departs from the GB relation ([Callynham et al. 2021](#)). Table 3 reports parameters, including brightness temperature, for our three VLITE detections of EI Cancri AB.

3. DISCUSSION

The VLITE detection of emission from EI Cancri AB represents the first confirmed detection of a UCD or UCD binary at ~ 340 MHz. Our results extend the known radio activity of EI Cancri AB to lower frequencies and suggest coherent emission in line with earlier M dwarfs observed at this frequency. However, incoherent emission cannot be ruled out without additional data. Here we discuss the possible mechanisms of the emission, additional emission in the 7-hour and full datasets, EI Cancri AB at higher frequencies, and the magnetic properties of the system.

3.1. Coherent Case: ECMI vs. Plasma Emission

In the case of coherent emission, we cannot directly distinguish between ECMI or plasma emission at this time using VLITE. However, radio-emitting UCDs have been shown to frequently exhibit coherent emission via the ECMI mechanism ([Hallinan et al. 2008; Villadsen & Hallinan 2019](#)). Thus, we suspect that the emission is from ECMI.

Distinguishing between ECMI and plasma emission is frequently done by analyzing the periodicity of the signal, how broadband the emission is, the frequency drift, and/or polarization properties of the emission (e.g., [Lynch et al. 2017; Villadsen & Hallinan 2019; Zic et al. 2019; Rose et al. 2023; Bloot et al. 2024; Callynham et al. 2024](#)). With only one epoch of detection, we are unable to identify a periodic signal. The VLITE band is also only ~ 40 MHz

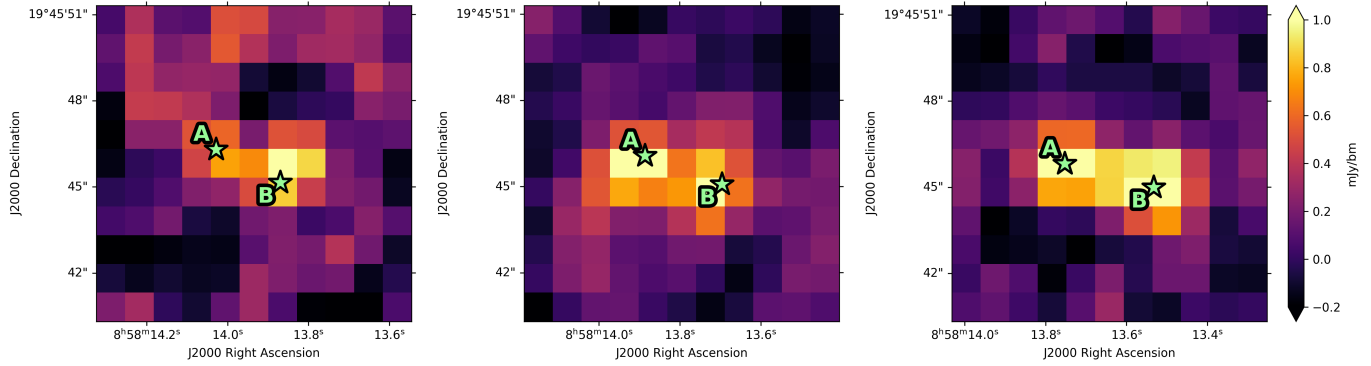


Figure 2. Detections of EI Cancri A and B during VLASS epochs 1, 2, and 3, i.e., in 2019, 2021, and 2024 (left to right). The positions of the stellar components are labeled, corrected for proper motion. Both stars are detected in all three epochs. See Table 2 for associated measurements and calculations.

wide; we detect emission in all three of its sub-bands for the combined 7-hour image. The band is not wide enough to place additional constraints on how broadband the emission is or to check for frequency drift, especially not without potentially diluting the signal below detectability in the time chopped images. VLITE has some polarization capability, but complexity in the VLITE system has hindered development of the analysis process; many studies use the circular polarization fraction to discern between emission mechanisms, but VLITE exhibits leakage between components and non-polarized light. Because VLITE is commensal with other VLA programs, the VLITE program has no control over calibrator observations, making it yet more difficult to disentangle the circular (V) and two linear (Q & U) polarization components. It is possible to extract a total polarization value, $P = \sqrt{Q^2 + U^2 + V^2}$; refinement of the process is underway to be presented in future work.

3.2. Incoherent Case: Synchrotron Radiation

Incoherent emission in the form of gyrosynchrotron radiation is common in other magnetically active M dwarfs. However, by evaluating the speed of the electrons, we reveal the possibility of synchrotron radiation. If our detected flux comes from a large loop at $5 R_*$, we can estimate 340 MHz brightness temperatures of $\sim 10^{11}$ K. If we examine the scenario of a region with high opacity, effective temperature is approximately equal to this brightness temperature. With this assumption, we can calculate a kinetic energy of 8.6 MeV per electron, corresponding to a Lorentz factor of 1.7. This would indicate relativistic speeds in the form of synchrotron radiation. Synchrotron emission from an ultracool dwarf is relatively novel, with only a few studies examining it, e.g., in the contexts of expanding plasma blobs (Vedantham et al. 2022) and radiation belts (Kao et al. 2023). Follow-up observations on this system are needed to discern whether synchrotron radiation is behind our detections, as described in Section 4.

3.3. Additional Emission at 340 MHz

The three VLITE detections were identified within a 7-hour image upon time chopping at a 10 minute cadence. However, we also identify a signal of $S/N = 7.7$ within the full, non-chopped, 7-hour image, with a peak flux of 2.70 ± 0.35 mJy corresponding to $T_B = 1.81 \times 10^{12}$ K $\pm 4.03 \times 10^{11}$ K. This begs the question of whether there is additional emission below our time-chop detection limits. Integrating the flux of the three detections across their 10-minute timescales and dividing by the full image time as in equation 3, we calculate an expected flux of 0.825 mJy during the 7-hour period, short of the flux from the actual 7-hour image. This result suggests additional flux below our sensitivity at the 10-minute cadence, but measurable in the combined image. Thus, we find that there is a low level of emission from EI Cancri A and/or B during the 2018 April epoch below our chopping detection limits.

$$f_{peak,3 \text{ detections}} = \frac{(f_{peak,1} + f_{peak,2} + f_{peak,3}) \tau_{chop}}{\tau_{7hr}} = 0.825 \text{ mJy} < f_{peak,7hr} = 2.70 \text{ mJy} \quad (3)$$

To search for quiescent emission, we combined images spanning 3-month intervals of VLITE data throughout the full dataset, excluding the 7-hour detection image. The time frame was chosen to be as long as possible without significant shifting due to proper motion. No emission outside the 2018 dates is detected, with 3σ limits that are typically 4 – 6

mJy bm^{-1} or higher. Thus, these combinations would not detect the 2.7 mJy emission measured in the 7-hour image from 2018. Combining the 7-hour detection image with other images taken in early 2018 lowers the measured flux, which suggests that the true quiescent level, if any, is even lower. Kao & Pineda (2025) find that UCD binaries are more likely to exhibit quiescent emission than single UCDs. Quiescent emission below our detection limit is unlikely to be driven by flares in the system, although the flares may populate the necessary charged particles (Kao et al. 2023).

3.4. Higher Frequency Emission, Magnetic Activity, and Rotation

Within the 31 years of published archival radio data, only resolved observations by the VLA Sky Survey (VLASS) reveal emission from both stars (see Figure 2). VLASS epoch 3 flux measurements have not yet been released; we extracted flux densities from the publicly available Quick Look image, adopting Canadian Initiative for Radio Astronomy Data Analysis (CIRADA)⁴ PyBDSF parameters to be consistent with the epoch 1 and 2 catalogs. We also force fit the VLASS 1 image for the A component, which was not reported in the data release. For all measurements, we scaled the peak flux values by 5% to account for flux bias⁵ and added 5% flux scale uncertainties to the error in quadrature (Perley & Butler 2017). Peak fluxes were adopted as flux density to account for fitting biases introduced by the presence of the companion. Brightness temperatures from all three epochs approach the 10^{12} K border between coherent and incoherent emission, expected to occur at a radius of $\sim R_*$. Incoherent emission may be gyrosynchrotron radiation tied to flares, given the frequent flares in the system. This would not be surprising for such a magnetically active system. However, given that our brightness temperatures are very close to 10^{12} K, this emission may actually be coherent.

As summarized in Table 2, EI Cancri AB has been detected at higher frequencies over the past three decades, with observations from 1993 to 2024 spanning 855.5 to 5000 MHz and extending into the microwave regime. Magnetic activity can drive these events and manifests across the electromagnetic spectrum. With an H_{α} equivalent width ($\text{EW}_{H_{\alpha}}$) of -5.719, this system is classified as “active,” according to Newton et al. (2017). We also observe signs of magnetic activity in the form of near- and far-ultraviolet emission (Galaxy Explorer; GALEX; Martin et al. 2005; Bianchi et al. 2017), X-ray emission (ROentgen SATellite; ROSAT; Boller et al. 2016), and frequent optical flaring and starspot modulation present in four sectors of TESS data (TESS Team 2018). Magnetically active stars often also produce gyrosynchrotron emission, especially during flaring events. However, we cannot identify whether the archival detections of this system are due to incoherent gyrosynchrotron emission.

Strongly tied to magnetic activity, we find multiple possible rotation periods for EI Cancri A and B in the literature. Jeffers et al. (2018)⁶ report a projected rotational velocity ($vsini$) of $16.70 \pm 0.64 \text{ km s}^{-1}$ for the system, which could correspond to a period upper limit of 10.76 hours for EI Cancri A or 9.60 hours for EI Cancri B. In contrast, a period of 83.270 days is measured by Newton et al. (2016), and we calculate rotation periods of 112.74 days and 115.53 days, respectively, for EI Cancri A and B using the Newton et al. (2017) mass-rotation relation. With the resolved observations from VLASS, we now know that both stars are magnetically active, rather than one or the other. This is notable because a 10-hour rotation period is compatible with expectations for a magnetically active M dwarf, while a rotational period of 83 days would be strikingly long. This is evidenced in the Newton et al. (2017) mass-rotation-activity diagram (Fig. 5), where a ~ 10 -hour period implies an active star, while an 83-day period suggests more likely inactivity (although the sample in that area of phase space is small). Similarly, we can estimate an X-ray to bolometric luminosity ratio for this system of $L_X/L_{bol} \sim 1.5 \times 10^{-3}$ (adopting $\log L_{bol} \sim -2.8$ based on Pecaut et al. 2012; Pecaut & Mamajek 2013)⁷ and find that it is consistent with the majority of fully convective stars at the shorter ~ 10 -hour period, versus uncharacteristically high at an 83-day period (see Figure 2 of Wright et al. 2018). Nevertheless, it is unclear what each period can be ascribed to in this system; it is possible that the two different timescales each correspond to a rotation period, with one star at ~ 10 hours and the other at 83 days. This would be an unusual mismatch between two otherwise similar stars in the same system and at odds with the detection of magnetic activity in both stars, as resolved by VLASS. However, discrepant rotation periods for more identically twin M dwarfs have been measured before by Couperus et al. (2025b,a), although the largest mismatch is 6.55 days and 38 days. To characterize the possible discrepancy between observed magnetic activity and stellar rotation rate in the EI Cancri system, a rotation period must be determined for each star via resolved observations.

⁴ <https://cirada.ca/>

⁵ see VLASS Project Memo #22

⁶ referencing Rodríguez, H. 2014, Master’s thesis, UCM Madrid

⁷ https://github.com/emamajek/SpectralType/blob/master/EEM_dwarf_UBVIJHK_colors_Teff.txt

3.5. Summary

Radio flux has been emitted from EI Cancri AB at 340 MHz, most likely through the ECMI process. Additional data are needed to discern between coherent and incoherent emission and to rule out plasma emission, gyrosynchrotron radiation, and synchrotron radiation at this frequency. The VLASS data provide the only published dataset for this system with resolved emission, revealing that both stars are radio emitters. We cannot deduce whether the VLASS emission is coherent or incoherent because the brightness temperature of each event approaches the 10^{12} K boundary. However, we suspect coherent emission in most cases because our brightness temperatures are lower limits. Meanwhile, additional emission of unknown origin has persisted across a broad range of higher radio frequencies for the past 3 decades. Adding a layer of intrigue to EI Cancri AB, the system has a visible light photometric signal with an 83-day period and a projected rotational velocity measurement corresponding to up to about 10 hours; while a 10-hour period aligns with other active M dwarf findings, the case of an 83-day rotation period for either star would be anomalous given their magnetic activity signatures.

4. CONCLUSIONS AND FUTURE WORK

We identify radio emission at 340 MHz from the EI Cancri system using VLITE, marking the first detection of an UCD at this frequency. To date, \sim 300-MHz frequency studies have detected only a handful of earlier-type M dwarfs. Since 1993, the EI Cancri system has been detected at higher frequencies, ranging from 855.5 MHz to 5.0 GHz and including microwave at 90–220 GHz. Expanding the detection frequency down to 340 MHz for the first time reveals that the ionized electrons extend further out from the stellar surface, suggesting a larger-scale magnetic field. Although we cannot disentangle which star is the emitter for each event, each event is point-like and is unlikely to be emission from both stars. Each of the three events could be either coherent or incoherent, depending on the radius of emission, which could be at the stellar disk or as far out on a magnetic loop as $\sim 5 R_*$. Based on findings at MHz frequencies for earlier M dwarfs, the emission is most likely coherent and auroral in nature, produced via the electron cyclotron maser instability mechanism, although we cannot presently rule out plasma emission, gyrosynchrotron radiation, or synchrotron radiation. This system is highly magnetically active, and incoherent emission is likely tied to flaring events. We detect no emission from VLITE during simultaneous TESS observations that reveal optical flares. EI Cancri also emits at 3 GHz, with resolved emission from both stars detected by VLASS confirming that both EI Cancri A and B are radio emitters.

To further characterize the nature of EI Cancri at 340 MHz will require additional data with higher sensitivity and broader wavelength and/or time coverage to track frequency drift and/or search for a periodic signal. One option is pointed observations using the VLA WIDAR system at P-band; centered at a similar frequency, the VLA WIDAR P-band system provides a wider bandpass than VLITE and therefore is more sensitive to fainter emission. Also, pointed, on-axis observations would not suffer the attenuation we correct for in our VLITE observations (0.874° from pointing center). In addition, without the effects of off-axis polarization leakage, we could properly calibrate Stokes parameters. Lastly, we would have access to the full 27 antennas in the array, rather than the 18 antennas used for VLITE. This would yield more collecting area and uv coverage. Summarily, pointed VLA observations in P-band could lead to higher S/N, polarization information, and improved time resolution of the rise and decay of events at \sim 300 MHz (see for example, [Villadsen & Hallinan 2019](#)). Another option is to take pointed GHz frequency observations using the VLA to be combined with simultaneous VLITE observations at 340 MHz. Refinement of the VLITE polarization data processing procedures could also yield a measurement of the polarization fraction for the detections reported in this paper to discern between emission mechanisms. Branching out to other facilities, Very Long Baseline Array⁸ observations could be acquired to map out the orbit of the system, while also probing ~ 300 MHz, with options ranging from P-band to 96 GHz. A spectrum using archival EI Cancri AB detections is challenging to interpret due to uncertainty in the fraction of emission coming from each component and in the time evolution of the emission. Resolved radio observations spanning a range of frequencies would facilitate the construction of a spectrum for each star. In this highly magnetically active system with multiple possible rotation periods, it would also be valuable to determine the rotation period of each star and identify whether they are uncharacteristically long (see Section 3.4). This could be done by measuring projected rotational velocity via high resolution infrared spectroscopy observations with a 1'' or smaller slit. Another compelling case is to observe the system using Keck adaptive optics with the infrared wavefront sensor. These data would provide resolved infrared flux measurements on each star and constrain the parameter space

⁸ <https://science.nrao.edu/facilities/vlba>

for any additional UCD components in the system. Critically, they could be used in understanding their full spectral properties and derive fundamental parameters such as effective temperature, bolometric luminosity, and radius, key to putting the star in context with the greater UCD population.

ACKNOWLEDGEMENTS

We thank Dr. Rachel Osten for insightful discussions on UCD magnetic activity at radio frequencies. We also thank our referee for their comments, which contributed to the interpretation of our results and improved the clarity of their presentation.

This scientific work uses data obtained from Inyarrimanha Ilgari Bundara / the Murchison Radio-astronomy Observatory. We acknowledge the Wajarri Yamaji People as the Traditional Owners and native title holders of the Observatory site. CSIRO's ASKAP radio telescope is part of the Australia Telescope National Facility (<https://ror.org/05qajvd42>). Operation of ASKAP is funded by the Australian Government with support from the National Collaborative Research Infrastructure Strategy. ASKAP uses the resources of the Pawsey Supercomputing Research Centre. Establishment of ASKAP, Inyarrimanha Ilgari Bundara, the CSIRO Murchison Radio-astronomy Observatory and the Pawsey Supercomputing Research Centre are initiatives of the Australian Government, with support from the Government of Western Australia and the Science and Industry Endowment Fund. This paper includes archived data obtained through the CSIRO ASKAP Science Data Archive, CASDA (<https://data.csiro.au>).

The National Radio Astronomy Observatory is a facility of the National Science Foundation operated under cooperative agreement by Associated Universities, Inc. CIRADA is funded by a grant from the Canada Foundation for Innovation 2017 Innovation Fund (Project 35999), as well as by the Provinces of Ontario, British Columbia, Alberta, Manitoba and Quebec.

This work has made use of data from the European Space Agency (ESA) mission *Gaia* (<https://www.cosmos.esa.int/gaia>), processed by the *Gaia* Data Processing and Analysis Consortium (DPAC, <https://www.cosmos.esa.int/web/gaia/dpac/consortium>). Funding for the DPAC has been provided by national institutions, in particular the institutions participating in the *Gaia* Multilateral Agreement.

This paper includes data collected with the TESS mission, obtained from the MAST data archive at the Space Telescope Science Institute (STScI). Funding for the TESS mission is provided by the NASA Explorer Program. STScI is operated by the Association of Universities for Research in Astronomy, Inc., under NASA contract NAS 5-26555.

This project was supported in part by an appointment to the NRC Research Associateship Program at the U.S. Naval Research Laboratory in Washington, D.C., administered by the Fellowships Office of the National Academies of Sciences, Engineering, and Medicine.

Basic research at NRL is funded by 6.1 Base programs. Construction and installation of VLITE was supported by the NRL Sustainment Restoration and Maintenance fund.

Facilities: VLITE, VLA, TESS, GALEX, ROSAT, Gaia, ACT, ASKAP

Software: Python, NumPy ([Harris et al. 2020](#)), Matplotlib ([Hunter 2007](#)), Astropy ([Astropy Collaboration et al. 2022](#)), Obit ([Cotton 2008](#)), AIPS ([Greisen 2003](#)), PyBDSF ([Mohan & Rafferty 2015](#))

REFERENCES

- Astropy Collaboration, Price-Whelan, A. M., Lim, P. L., et al. 2022, ApJ, 935, 167, doi: [10.3847/1538-4357/ac7c74](https://doi.org/10.3847/1538-4357/ac7c74)
- Babusiaux, C., Fabricius, C., Khanna, S., et al. 2023, A&A, 674, A32, doi: [10.1051/0004-6361/202243790](https://doi.org/10.1051/0004-6361/202243790)
- Bailer-Jones, C. A. L., Rybizki, J., Fouesneau, M., Demleitner, M., & Andrae, R. 2021, AJ, 161, 147, doi: [10.3847/1538-3881/abdf806](https://doi.org/10.3847/1538-3881/abdf806)
- Bastian, T. S., Benz, A. O., & Gary, D. E. 1998, ARA&A, 36, 131, doi: [10.1146/annurev.astro.36.1.131](https://doi.org/10.1146/annurev.astro.36.1.131)
- Becker, R. H., White, R. L., & Helfand, D. J. 1995, ApJ, 450, 559, doi: [10.1086/176166](https://doi.org/10.1086/176166)
- Belokurov, V., Penoyre, Z., Oh, S., et al. 2020, MNRAS, 496, 1922, doi: [10.1093/mnras/staa1522](https://doi.org/10.1093/mnras/staa1522)
- Benz, A. O., & Guedel, M. 1994, A&A, 285, 621
- Berger, E. 2006, ApJ, 648, 629, doi: [10.1086/505787](https://doi.org/10.1086/505787)
- Bianchi, L., Shiao, B., & Thilker, D. 2017, ApJS, 230, 24, doi: [10.3847/1538-4365/aa7053](https://doi.org/10.3847/1538-4365/aa7053)

- Bloot, S., Callingham, J. R., Vedantham, H. K., et al. 2024, *A&A*, 682, A170, doi: [10.1051/0004-6361/202348065](https://doi.org/10.1051/0004-6361/202348065)
- Boller, T., Freyberg, M. J., Trümper, J., et al. 2016, *A&A*, 588, A103, doi: [10.1051/0004-6361/201525648](https://doi.org/10.1051/0004-6361/201525648)
- Bower, G. C., Bolatto, A., Ford, E. B., & Kalas, P. 2009, *ApJ*, 701, 1922, doi: [10.1088/0004-637X/701/2/1922](https://doi.org/10.1088/0004-637X/701/2/1922)
- Callingham, J. R., Vedantham, H. K., Shimwell, T. W., et al. 2021, *Nature Astronomy*, 5, 1233, doi: [10.1038/s41550-021-01483-0](https://doi.org/10.1038/s41550-021-01483-0)
- Callingham, J. R., Pope, B. J. S., Kavanagh, R. D., et al. 2024, *Nature Astronomy*, 8, 1359, doi: [10.1038/s41550-024-02405-6](https://doi.org/10.1038/s41550-024-02405-6)
- Callingham, J. R., Tasse, C., Keers, R., et al. 2025, arXiv e-prints, arXiv:2511.09289. <https://arxiv.org/abs/2511.09289>
- Cohen, A. S., Röttgering, H. J. A., Kassim, N. E., et al. 2003, *ApJ*, 591, 640, doi: [10.1086/375397](https://doi.org/10.1086/375397)
- Condon, J. J., Cotton, W. D., Greisen, E. W., et al. 1998, *AJ*, 115, 1693, doi: [10.1086/300337](https://doi.org/10.1086/300337)
- Cook, B. A., Williams, P. K. G., & Berger, E. 2014, *ApJ*, 785, 10, doi: [10.1088/0004-637X/785/1/10](https://doi.org/10.1088/0004-637X/785/1/10)
- Cotton, W. D. 2008, *PASP*, 120, 439, doi: [10.1086/586754](https://doi.org/10.1086/586754)
- Couperus, A. A., Henry, T. J., Kar, A., et al. 2025a, arXiv e-prints, arXiv:2510.22093, doi: [10.48550/arXiv.2510.22093](https://doi.org/10.48550/arXiv.2510.22093)
- Couperus, A. A., Henry, T. J., Osten, R. A., et al. 2025b, *AJ*, 169, 41, doi: [10.3847/1538-3881/ad9252](https://doi.org/10.3847/1538-3881/ad9252)
- Crosley, M. K., & Osten, R. A. 2018a, *ApJ*, 856, 39, doi: [10.3847/1538-4357/aaaec2](https://doi.org/10.3847/1538-4357/aaaec2)
- . 2018b, *ApJ*, 862, 113, doi: [10.3847/1538-4357/aacf02](https://doi.org/10.3847/1538-4357/aacf02)
- Drake, S. A., Simon, T., & Linsky, J. L. 1989, *ApJS*, 71, 905, doi: [10.1086/191402](https://doi.org/10.1086/191402)
- Driessen, L. N., Pritchard, J., Murphy, T., et al. 2024, *PASA*, 41, e084, doi: [10.1017/pasa.2024.72](https://doi.org/10.1017/pasa.2024.72)
- Duchesne, S. W., Grundy, J. A., Heald, G. H., et al. 2024, *PASA*, 41, e003, doi: [10.1017/pasa.2023.60](https://doi.org/10.1017/pasa.2023.60)
- Duchesne, S. W., Ross, K., Thomson, A. J. M., et al. 2025, *PASA*, 42, e038, doi: [10.1017/pasa.2025.2](https://doi.org/10.1017/pasa.2025.2)
- Dulk, G. A. 1985, *ARA&A*, 23, 169, doi: [10.1146/annurev.aa.23.090185.001125](https://doi.org/10.1146/annurev.aa.23.090185.001125)
- Gaia Collaboration. 2022, Gaia Data Release 3 (Gaia DR3), European Space Agency, doi: [10.5270/esa-qa4lep3](https://doi.org/10.5270/esa-qa4lep3)
- Gaia Collaboration, Prusti, T., de Bruijne, J. H. J., et al. 2016, *A&A*, 595, A1, doi: [10.1051/0004-6361/201629272](https://doi.org/10.1051/0004-6361/201629272)
- Gaia Collaboration, Vallenari, A., Brown, A. G. A., et al. 2023, *A&A*, 674, A1, doi: [10.1051/0004-6361/202243940](https://doi.org/10.1051/0004-6361/202243940)
- Greisen, E. W. 2003, in *Astrophysics and Space Science Library*, Vol. 285, *Information Handling in Astronomy - Historical Vistas*, ed. A. Heck, 109, doi: [10.1146/annurev.aa.29.090191.000335](https://doi.org/10.1146/annurev.aa.29.090191.000335)
- Guedel, M., & Benz, A. O. 1993, *ApJL*, 405, L63, doi: [10.1086/186766](https://doi.org/10.1086/186766)
- Hallinan, G., Antonova, A., Doyle, J. G., et al. 2008, *ApJ*, 684, 644, doi: [10.1086/590360](https://doi.org/10.1086/590360)
- Harris, C. R., Millman, K. J., van der Walt, S. J., et al. 2020, *Nature*, 585, 357, doi: [10.1038/s41586-020-2649-2](https://doi.org/10.1038/s41586-020-2649-2)
- Helfand, D. J., White, R. L., & Becker, R. H. 2015, *ApJ*, 801, 26, doi: [10.1088/0004-637X/801/1/26](https://doi.org/10.1088/0004-637X/801/1/26)
- Huang, Q., Jiang, B., Zhang, Z., & Zijlstra, A. 2024, *ApJ*, 977, 50, doi: [10.3847/1538-4357/ad8b25](https://doi.org/10.3847/1538-4357/ad8b25)
- Hunter, J. D. 2007, *Computing in Science & Engineering*, 9, 90, doi: [10.1109/MCSE.2007.55](https://doi.org/10.1109/MCSE.2007.55)
- Hurley-Walker, N., Galvin, T. J., Duchesne, S. W., et al. 2022, *PASA*, 39, e035, doi: [10.1017/pasa.2022.17](https://doi.org/10.1017/pasa.2022.17)
- Jaeger, T. R., Osten, R. A., Lazio, T. J., Kassim, N., & Mutel, R. L. 2011, *AJ*, 142, 189, doi: [10.1088/0004-6256/142/6/189](https://doi.org/10.1088/0004-6256/142/6/189)
- Jeffers, S. V., Schöfer, P., Lamert, A., et al. 2018, *A&A*, 614, A76, doi: [10.1051/0004-6361/201629599](https://doi.org/10.1051/0004-6361/201629599)
- Kao, M. M., Hallinan, G., & Pineda, J. S. 2019, *MNRAS*, 487, 1994, doi: [10.1093/mnras/stz1372](https://doi.org/10.1093/mnras/stz1372)
- Kao, M. M., Hallinan, G., Pineda, J. S., et al. 2016, *ApJ*, 818, 24, doi: [10.3847/0004-637X/818/1/24](https://doi.org/10.3847/0004-637X/818/1/24)
- Kao, M. M., Mioduszewski, A. J., Villadsen, J., & Shkolnik, E. L. 2023, *Nature*, 619, 272, doi: [10.1038/s41586-023-06138-w](https://doi.org/10.1038/s41586-023-06138-w)
- Kao, M. M., & Pineda, J. S. 2025, *MNRAS*, 539, 2292, doi: [10.1093/mnras/stae905](https://doi.org/10.1093/mnras/stae905)
- Kavanagh, R. D., Vedantham, H. K., Rose, K., & Bloot, S. 2024, *A&A*, 692, A66, doi: [10.1051/0004-6361/202452094](https://doi.org/10.1051/0004-6361/202452094)
- Kirkpatrick, J. D., Henry, T. J., & Irwin, M. J. 1997, *AJ*, 113, 1421, doi: [10.1086/118357](https://doi.org/10.1086/118357)
- Lacy, M., Baum, S. A., Chandler, C. J., et al. 2020, *PASP*, 132, 035001, doi: [10.1088/1538-3873/ab63eb](https://doi.org/10.1088/1538-3873/ab63eb)
- Li, Y., Biermann, E., Naess, S., et al. 2023, *ApJ*, 956, 36, doi: [10.3847/1538-4357/ace599](https://doi.org/10.3847/1538-4357/ace599)
- Lindgren, L., Hernández, J., Bombrun, A., et al. 2018, *A&A*, 616, A2, doi: [10.1051/0004-6361/201832727](https://doi.org/10.1051/0004-6361/201832727)
- Lynch, C. R., Lenc, E., Kaplan, D. L., Murphy, T., & Anderson, G. E. 2017, *ApJL*, 836, L30, doi: [10.3847/2041-8213/aa5ffd](https://doi.org/10.3847/2041-8213/aa5ffd)
- Martin, D. C., Fanson, J., Schiminovich, D., et al. 2005, *ApJL*, 619, L1, doi: [10.1086/426387](https://doi.org/10.1086/426387)
- McConnell, D., Hale, C. L., Lenc, E., et al. 2020, *PASA*, 37, e048, doi: [10.1017/pasa.2020.41](https://doi.org/10.1017/pasa.2020.41)
- Melrose, D. B. 1991, *ARA&A*, 29, 31, doi: [10.1146/annurev.aa.29.090191.000335](https://doi.org/10.1146/annurev.aa.29.090191.000335)
- Mohan, A., Mondal, S., Wedemeyer, S., & Gopalswamy, N. 2024, *A&A*, 686, A51, doi: [10.1051/0004-6361/202347924](https://doi.org/10.1051/0004-6361/202347924)

- Mohan, N., & Rafferty, D. 2015, PyBDSF: Python Blob Detection and Source Finder, *Astrophysics Source Code Library*, record ascl:1502.007
- Murphy, T., & Kaplan, D. L. 2025, arXiv e-prints, arXiv:2511.10785. <https://arxiv.org/abs/2511.10785>
- Newton, E. R., Charbonneau, D., Irwin, J., et al. 2014, AJ, 147, 20, doi: [10.1088/0004-6256/147/1/20](https://doi.org/10.1088/0004-6256/147/1/20)
- Newton, E. R., Irwin, J., Charbonneau, D., et al. 2017, ApJ, 834, 85, doi: [10.3847/1538-4357/834/1/85](https://doi.org/10.3847/1538-4357/834/1/85)
- . 2016, ApJ, 821, 93, doi: [10.3847/0004-637X/821/2/93](https://doi.org/10.3847/0004-637X/821/2/93)
- Ortiz Ceballos, K. N., Cendes, Y., Berger, E., & Williams, P. K. G. 2024, AJ, 168, 127, doi: [10.3847/1538-3881/ad58be](https://doi.org/10.3847/1538-3881/ad58be)
- Pecaut, M. J., & Mamajek, E. E. 2013, ApJS, 208, 9, doi: [10.1088/0067-0049/208/1/9](https://doi.org/10.1088/0067-0049/208/1/9)
- Pecaut, M. J., Mamajek, E. E., & Bubar, E. J. 2012, ApJ, 746, 154, doi: [10.1088/0004-637X/746/2/154](https://doi.org/10.1088/0004-637X/746/2/154)
- Perley, R. A., & Butler, B. J. 2017, ApJS, 230, 7, doi: [10.3847/1538-4365/aa6df9](https://doi.org/10.3847/1538-4365/aa6df9)
- Pettersen, B. R. 1985, A&A, 148, 151
- Pineda, J. S., & Villadsen, J. 2023, Nature Astronomy, 7, 569, doi: [10.1038/s41550-023-01914-0](https://doi.org/10.1038/s41550-023-01914-0)
- Pineda, J. S., Youngblood, A., & France, K. 2021, ApJ, 918, 40, doi: [10.3847/1538-4357/ac0aea](https://doi.org/10.3847/1538-4357/ac0aea)
- Polisensky, E., Clarke, T. E., Giacintucci, S., & Peters, W. 2024, *Frontiers in Astronomy and Space Sciences*, 11, 1497375, doi: [10.3389/fspas.2024.1497375](https://doi.org/10.3389/fspas.2024.1497375)
- Polisensky, E., Richards, E., Clarke, T., Peters, W., & Kassim, N. 2019, in *Astronomical Society of the Pacific Conference Series*, Vol. 523, *Astronomical Data Analysis Software and Systems XXVII*, ed. P. J. Teuben, M. W. Pound, B. A. Thomas, & E. M. Warner, 441
- Polisensky, E., Lane, W. M., Hyman, S. D., et al. 2016, ApJ, 832, 60, doi: [10.3847/0004-637X/832/1/60](https://doi.org/10.3847/0004-637X/832/1/60)
- Ricker, G. R., Winn, J. N., Vanderspek, R., et al. 2015, *Journal of Astronomical Telescopes, Instruments, and Systems*, 1, 014003, doi: [10.1117/1.JATIS.1.1.014003](https://doi.org/10.1117/1.JATIS.1.1.014003)
- Rose, K., Pritchard, J., Murphy, T., et al. 2023, ApJL, 951, L43, doi: [10.3847/2041-8213/ace188](https://doi.org/10.3847/2041-8213/ace188)
- Route, M., & Wolszczan, A. 2013, ApJ, 773, 18, doi: [10.1088/0004-637X/773/1/18](https://doi.org/10.1088/0004-637X/773/1/18)
- Salama, M., Ziegler, C., Baranec, C., et al. 2022, AJ, 163, 200, doi: [10.3847/1538-3881/ac53fc](https://doi.org/10.3847/1538-3881/ac53fc)
- Stassun, K. G., & Torres, G. 2021, ApJL, 907, L33, doi: [10.3847/2041-8213/abdaad](https://doi.org/10.3847/2041-8213/abdaad)
- Tang, J., Tsai, C.-W., & Li, D. 2022, *Research in Astronomy and Astrophysics*, 22, 065013, doi: [10.1088/1674-4527/ac66bd](https://doi.org/10.1088/1674-4527/ac66bd)
- TESS Team. 2018, *TESS Input Catalog and Candidate Target List*, STScI/MAST, doi: [10.17909/FWDT-2X66](https://doi.org/10.17909/FWDT-2X66)
- Tokovinin, A., Mason, B. D., Mendez, R. A., Costa, E., & Horch, E. P. 2020, AJ, 160, 7, doi: [10.3847/1538-3881/ab91c1](https://doi.org/10.3847/1538-3881/ab91c1)
- van Haarlem, M. P., Wise, M. W., Gunst, A. W., et al. 2013, A&A, 556, A2, doi: [10.1051/0004-6361/201220873](https://doi.org/10.1051/0004-6361/201220873)
- Vedantham, H. K., Callingham, J. R., Shimwell, T. W., et al. 2022, ApJL, 926, L30, doi: [10.3847/2041-8213/ac5115](https://doi.org/10.3847/2041-8213/ac5115)
- . 2020, *Nature Astronomy*, 4, 577, doi: [10.1038/s41550-020-1011-9](https://doi.org/10.1038/s41550-020-1011-9)
- Vidotto, A. A., Jardine, M., Morin, J., et al. 2014, MNRAS, 438, 1162, doi: [10.1093/mnras/stt2265](https://doi.org/10.1093/mnras/stt2265)
- Villadsen, J., & Hallinan, G. 2019, ApJ, 871, 214, doi: [10.3847/1538-4357/aaef8e](https://doi.org/10.3847/1538-4357/aaef8e)
- Vrijmoet, E. H., Tokovinin, A., Henry, T. J., et al. 2022, AJ, 163, 178, doi: [10.3847/1538-3881/ac52f6](https://doi.org/10.3847/1538-3881/ac52f6)
- Vršnak, B., & Cliver, E. W. 2008, SoPh, 253, 215, doi: [10.1007/s11207-008-9241-5](https://doi.org/10.1007/s11207-008-9241-5)
- Williams, P. K. G., Cook, B. A., & Berger, E. 2014, ApJ, 785, 9, doi: [10.1088/0004-637X/785/1/9](https://doi.org/10.1088/0004-637X/785/1/9)
- Winters, J. G., Charbonneau, D., Henry, T. J., et al. 2021, AJ, 161, 63, doi: [10.3847/1538-3881/abcc74](https://doi.org/10.3847/1538-3881/abcc74)
- Wright, N. J., Newton, E. R., Williams, P. K. G., Drake, J. J., & Yadav, R. K. 2018, MNRAS, 479, 2351, doi: [10.1093/mnras/sty1670](https://doi.org/10.1093/mnras/sty1670)
- Zic, A., Stewart, A., Lenc, E., et al. 2019, MNRAS, 488, 559, doi: [10.1093/mnras/stz1684](https://doi.org/10.1093/mnras/stz1684)
- Zic, A., Murphy, T., Lynch, C., et al. 2020, ApJ, 905, 23, doi: [10.3847/1538-4357/abca90](https://doi.org/10.3847/1538-4357/abca90)